LBL-25743
Preprint

Lawrence Berkeley Laboratory
UNIVERSITY OF CALIFORNIA

DEC 2 1988

Submitted to Nuclear Physics A

Complex-Fragment Emission in 12.6 MeV/Nucleon ^{63}Cu Induced Reactions on ^{12}C and ^{27}Al Targets

H.Y. Han, K.X. Jing, E. Plagnol, D.R. Bowman,
R.J. Charity, L. Vinet, G.J. Wozniak,
and L.G. Moretto

August 1988

NUCLEAR SCIENCE DIVISION

Prepared for the U.S. Department of Energy under Contract Number DE-AC03-76SF00098.

LBL-25743 c.2

DISCLAIMER

This document was prepared as an account of work sponsored by the United States Government. While this document is believed to contain correct information, neither the United States Government nor any agency thereof, nor the Regents of the University of California, nor any of their employees, makes any warranty, express or implied, or assumes any legal responsibility for the accuracy, completeness, or usefulness of any information, apparatus, product, or process disclosed, or represents that its use would not infringe privately owned rights. Reference herein to any specific commercial product, process, or service by its trade name, trademark, manufacturer, or otherwise, does not necessarily constitute or imply its endorsement, recommendation, or favoring by the United States Government or any agency thereof, or the Regents of the University of California. The views and opinions of authors expressed herein do not necessarily state or reflect those of the United States Government or any agency thereof or the Regents of the University of California.

LBL - 25743

Complex-Fragment Emission in 12.6 MeV/Nucleon ^{63}Cu Induced Reactions on ^{12}C and ^{27}Al Targets

H. Y. Han[a], K. X. Jing[a], E. Plagnol[b], D. R. Bowman, R. J. Charity[c], L. Vinet[d], G. J. Wozniak, and L. G. Moretto

Nuclear Science Division, Lawrence Berkeley Laboratory, University of California, Berkeley, California 94720

Abstract: Complex fragments from the 12.6 MeV/nucleon ^{63}Cu + ^{12}C, ^{27}Al reactions were investigated. For both systems a projectile-like and/or a target-like component was observed along with an isotropic component. The roles of quasi elastic/deep inelastic processes, of statistical complex-fragment emission, and of the evaporation residue are discussed.

NUCLEAR REACTIONS: ^{12}C, ^{27}Al(^{63}Cu, Z), E = 12.6 MeV/nucleon; measured

E fragment σ(fragment, E_z, θ), fragment - fragment coincidence; deduced reaction mechanism. Statistical model calculations.

[a]Permanent address: Institute of Atomic Energy, Beijing, China.

[b]Present address: GANIL, B.P. 5027 - 14021 Caen Cedex, FRANCE.

[c]Present address: Gesellschaft für Schwerionenforschung, 6100 Darmstadt, West Germany

[d]Present address: CERN, Division EP, Ch-1211, Geneva 23, Switzerland.

1. Introduction

Complex fragments are very commonly associated with heavy ion reactions at low, intermediate and high energies. Despite their abundance in the latter two regimes, their origin is unclear and the subject of heated debate. At low energies, the following three sources: quasi-elastic/deep-inelastic reactions, evaporation residues and compound nucleus binary decay seem to be well established. Futhermore, their role at higher energies is slowly beginning to be recognized.[1-4]

Quasi-elastic and deep-inelastic reactions are perhaps the most common sources of complex fragments. In these processes the fragments are produced as the binary decay products of transient dinuclear structures originating from the target-projectile combination. This dinuclear structure, or dinuclear complex diffuses along the mass asymmetry coordinate. The longer the interaction time, the deeper is the energy relaxation, the more isotropic the angular distribution and the broader the product distribution in mass asymmetry. This process was the subject of intense study in the early seventies,[5-7] was somehow forgotten, and was recently resurrected as "orbiting"[8] for reactions in lighter systems. At intermediate energies this process is also well established in heavy symmetric systems[9] like ^{100}Mo + ^{100}Mo. Recently, it has been shown that the so called intermediate velocity source of complex fragments observed in the reaction 27 MeV/u ^{40}Ar + ^{nat}Ag was in fact associated with binary quasi- and deep-inelastic reactions.[10]

Highly excited light compound nuclei frequently produce evaporation residues far removed in mass and charge from the original compound nucleus by extensive light particle evaporation. Because of this massive evaporation, these residues may not be easily identified as such from their perturbed kinematic signature and may be confused with fragments arising from other sources.

More recently, it has been shown that complex fragments can be emitted by compound nuclei in a statistical binary decay.[11-17] This process is best understood by considering the ordinary light particle evaporation on the one hand, and fission on the other as the extreme forms of a common process, whose underlying connection is provided by the mass-asymmetry coordinate. The modulation of the potential energy

along the mass-asymmetry coordinate is responsible for the strong variation of the cross sections with mass asymmetry. The relationship between the yield Y and the potential energy V(asym) is approximately $Y \propto \exp[-V(asym)/T]$ where T is the temperature. As the excitation energy increases, the role of the potential energy diminishes and the fragment yields tend to become more nearly equal. The approximate dependence of the potential energy and the yield upon mass asymmetry is shown in Fig. 1 for two nuclei, one above and one below the Businaro-Gallone point. For a heavy compound nucleus, the mass distribution shows a peak at symmetry (fission peak) and two wings at extreme asymmetries (evaporation wings). For a light system, the peak at symmetry disappears, and is replaced by a minimum creating a U-shaped mass distribution.[18]

At intermediate and high energies the yields from the quasi-elastic/deep inelastic, evaporation residues, and the compound nucleus binary decay processes may overlap to such an extent as to create at times a mess difficult to untangle (see Fig. 2). The premature discovery of multifragmentation and liquid vapor equilibrium can be attributed to these complications. This confusion can be obviated by taking simple precautions. For instance the second process (evaporation residues) can be isolated by choosing a sufficiently heavy target (or projectile), thus confining the evaporation residues to relatively large masses. Similarly, the first (quasi-elastic/deep-inelastic) and third (compound nucleus binary decay) processes can be distinguished by choosing a sufficiently asymmetric system so that a good portion of the range between the target and projectile is free from quasi-elastic and deep-inelastic processes and is populated mainly by compound nucleus decay. Recently the role of these components has been clearly illustrated in a series of studies covering a very broad energy range by means of reverse kinematics reactions.[13-16] This technique has proven to be invaluable because of the ease of identification of all the fragments and of the narrow angular range that needs to be covered in order to catch them all.

In very light systems (e.g. $^{40}Ar + ^{27}Al$, etc.) all three components become substantially mixed[19], even at relatively low energies, for a variety of reasons (see Fig. 2). For instance:

1. Evaporation residues resulting from conventional evaporation (neutron and light

charged particle) can reach very light masses.

2. The entrance-channel mass asymmetry may not leave enough room (mass range between target and projectile) for the compound nucleus products to appear without a substantial deep inelastic contamination.
3. The small Coulomb field does not provide enough "kick" to the heavier binary fragments so that they can not be readily distinguished from the evaporation residues.

As a consequence, what may be a reasonably clear environment for a heavier system, may be a very messy one for a lighter system. On the other hand, it may be profitable to study relatively light systems in order to extend our knowledge of the conditional barriers associated with compound nucleus decay.

We have attempted to recover some of the simplicities of the heavy systems in the light mass region by studying two systems which are sufficiently light to portray some of the difficulties discussed above, but which are manageable in terms of Coulomb energies and mass asymmetries. The reactions chosen were ^{63}Cu + ^{12}C, ^{27}Al at 12.6 MeV/u and they have been studied with the reverse kinematics technique.

In section 2 the experimental technique is described. The results are presented in section 3. The conclusions are contained in section 4.

2. Experimental Method

This experiment was performed at the 88-Inch Cyclotron of Lawrence Berkeley Laboratory. An ECR source was utilized to produce $^{63}Cu^{19+}$ ions which after injection into the cyclotron and acceleration to 12.6 MeV/A, impinged on the targets of ^{12}C (413 $\mu g/cm^2$) and ^{27}Al (496 $\mu g/cm^2$).

Two position-sensitive ΔE-E quad telescopes were used to detect the fragments emitted in the reactions. Each quad unit consisted of four separate gas-silicon telescopes which covered 25° degrees in plane and 5° degrees out-of-plane. The active area of each telescope subtended 5.0^o and the separation between each telescope was 1.6^o. These telescopes were designed to get into small angles ($\sim 4^o$) relative to the beam so that complete angular distributions could be measured for reverse kinematics reactions. The gas ionization detectors served as ΔE detectors and

were operated at a pressure of 40 torr of CF_4 gas. The E detectors in each telescope unit were 5 x 5 cm^2 square (5mm thick) silicon detectors with a resistive layer on the front to determine the position. Using these telescopes, the energy, the atomic number, the in-plane and out-of-plane angles could be determined for each fragment that traversed the ΔE and stopped in the E detector. The out-of-plane angle of the incident particle was determined from the drift time in the gas ionization detector and the in-plane angle was determined from a resistive division of the energy signal from the silicon detector. These telescopes were designed to measure continuous angular distributions over 25° lab intervals by overlapping the two quad units so that the dead areas between telescopes was covered. In this way, complete and continuous angular distributions could be obtained for constructing invariant cross section diagrams in a relatively short amount of beam time.

The atomic charge of the detected particles was determined from the measured ΔE and E values. Examples of ΔE-E spectra illustrating the range of fragments observed and the Z resolution achieved are shown in Fig. 3. In this figure, one clearly sees the upper and lower kinematic ridges associated with the binary decay of a fast moving compound nucleus. The upper ridge corresponds to fragments emitted forward in the c.m. system and the lower ridge to fragments emitted backward in the c.m. system.

The energy calibrations of the E and ΔE detectors and the position calibrations were performed using the method illustrated in Ref. 16. The energy calibrations were accurate to ±1% and the position resolution obtained was $\pm 0.2^o$. The absolute cross sections were determined from the beam charge collected in a Faraday cup. The charge state of ^{63}Cu ions entering the Faraday cup was determined by means of elastic scattering on a ^{197}Au target with thickness of 40 $\mu g/cm^2$.

All the data, both inclusive and coincidence events between two or more detector telescopes were recorded on magnetic tape and analyzed off line.

3. Experimental Results

3.1 Velocity Diagrams

Inspection of the ΔE-E map shown in Fig. 3, reveals that for each atomic number the fragment kinetic energy spectrum presents two distinct peaks. This can be seen better

by transforming this and similar ΔE-E spectra into Z-V contour diagrams. The velocity V of a fragment can be calculated from its energy and mass. The mass of a fragment, A, can be determined from its measured atomic number using the empirical formula,[16]

$$A = 2.08Z + 0.0029Z^2 \qquad (1)$$

where Z is the measured atomic number of the fragment. When the excitation energy of a fragment is greater than 1 MeV/u, the above formula predicts its average mass number with an accuracy of ± 0.5 amu for Z values between $5 \leq Z \leq 40$. In Fig. 4, we give some examples of the cross section $\partial^2\sigma/\partial V\partial Z$ plotted in the Z - V plane for four different laboratory angles. For each Z-value, one observes two distinct velocities which form a high and low velocity ridge, which for large Z-values converge to form a Λ pattern. The separation between the two ridges corresponds to the Coulomb velocities expected in a binary decay as observed at the angle indicated in the figures. The two components correspond to the two kinematic solutions arising from reverse kinematics. One solution corresponds to the fragment going forward in the source frame with Coulomb velocity and the other corresponds to the fragment going backward with the same c.m. velocity. In the laboratory frame both fragments are observed at the same angle but with different velocities. As one progresses toward the kinematic limits, the Λ pattern shrinks as θ_{lab} increases.

A more effective way to visualize the source(s) of complex fragments is to plot the cross section $\partial^2\sigma/\partial V_\perp\partial V_{||}$ in the $V_{||}$ - $V_\perp$ plane for each atomic number. Typical linear contour plots of this cross section for the ^{63}Cu + ^{12}C,^{27}Al reactions for various Z-species are given in Fig. 5 and Fig. 6, respectively. The dashed lines in the figures show the minimum angles covered by the telescopes and their velocity thresholds. For most Z-values, complete and continuous angular distributions have been obtained. Such distributions are very helpful in obtaining a global picture of the reaction. The cross sections were measured from 5° to 72° in the laboratory system, which is adequate to obtain complete angular distributions.

These cross section plots have the following main features.

1. A ring of high cross section (Coulomb ring) is visible in all plots. In contrast the central region is characterized by an absence of events. The Coulomb ring corresponds to the emission of fragments with Coulomb-like velocities from a single source with a well defined laboratory velocity.
2. The radius of the Coulomb velocity rings, corresponding to the emission velocity with which the complex fragments are emitted in the source frame, becomes smaller and smaller with increasing atomic number. This behaviour is simply due to momentum conservation in a Coulomb controlled binary decay.
3. An isotropic component seems to be present for all atomic numbers. The intensity of this component can be seen from the density of the contours.
4. For atomic numbers near those of the target and projectile, one observes anisotropic components as well as incompletely relaxed components.

The first and second features are indications of fully relaxed binary decays associated with either deep-inelastic processes or compound-nucleus emission. The source of these fragments can be characterized by its velocity which can be extracted from the centers of the Coulomb circles following the method presented in Ref. 16. The source velocities vs. fragment atomic number for both reactions are shown in Fig. 7. These source velocities are independent of atomic number and agree closely with the velocity expected for complete fusion, also shown in the figure.

The radii of the Coulomb circles and the variances are also shown in Fig. 7. The Coulomb nature of these velocities can be inferred from their magnitude and from their nearly linear dependence with atomic number. A calculation of the Coulomb velocities based upon the Viola systematics[20] generalized to asymmetric divisions and corrected for sequential decay is also shown (dashed line) in the figure. The addition of angular momentum effects produces the solid lines which appear to be in excellent agreement with the data. One should note that for a given Z value, the velocities are somewhat larger for the heavier $^{63}Cu + ^{27}Al$ system than the $^{63}Cu + ^{12}C$ system. This is due to the fact that the Coulomb energy is higher in the former system and that, for a given

Z-value, momentum conservation lends greater velocity to the light fragment in the heavier system.

The third feature indicates on one hand the presence of an isotropic component which one is tempted to assign to compound nucleus decay. The fourth feature consisting of the anisotropic components, by their nearness in Z-value to the target and/or projectile is characteristic of quasi and deep inelastic processes.

3.2 Angular Distribution

In the previous section, it was pointed out that the target-like and projectile-like components along with an isotropic component are visible in some of the velocity diagrams. The experimental angular distributions of complex fragments may provide an opportunity to isolate the contribution of the various components. The $d\sigma/d\theta$ distributions in the frame of the source system were extracted from the data for all the identified fragments. These angular distributions are shown in Fig. 8.

In the case of $^{63}Cu + ^{12}C$ the distributions are peaked at backward angles for fragment Z-values less than 10 due to the presence of the target-like quasi-elastic and deep-inelastic components, while the distributions for Z>21 show a forward peaking associated with the projectile-like component. At intermediate Z-values, the angular distributions are almost flat, strongly suggesting that a compound nucleus component is present. Thus we can assume that the angular distribution includes an isotropic component for all Z-values.

Similar features are also observed in Fig. 8 for the $^{63}Cu + ^{27}Al$ reaction. However, the transition from backward to forward peaking is rather abrupt, leaving only two or three Z-values (13, 14, 15) with a nearly isotropic angular distribution. The reason for this is probably associated with the more symmetric entrance channel of this reaction which leads to a near overlap of the target and projectile-like components of the deep-inelastic processes (see Fig. 2). Consequently, in this reaction the extraction of the compound nucleus component is somewhat complicated by the large yield of the quasi-elastic and deep-inelastic components in the forward or backward angular regions.

The backward peaking in the angular distributions of both reactions is more

accentuated in the general vicinity of the target atomic number. This is especially visible for the $^{63}Cu + ^{27}Al$ reaction where the backward peaking is seen to increase from Z = 4 to Z = 8,9 and to decrease again until it disappears at about Z = 12,13. The backward peaking is not strongest at Z = 13 presumably because of secondary charge loss by the target-like fragment. This feature should be complemented by the forward peaking of the projectile-like fragment. While the forward peaking is indeed observed, fragments larger than the projectile Z value were not detected in the angular range studied due to the strong kinematic forward focusing.

The observed behavior of the quasi-elastic and deep-inelastic components fits well within the diffusion picture developed more than a decade ago and is in agreement with the experimental observations in similar reaction studied in normal kinematics.[21-24]

3.3 Cross Section

As mentioned above, isotropic components can be seen for many fragment Z-values in both reactions. Therefore, one can attempt to separate the isotropic from the anisotropic component in the angular distributions and obtain the angle-integrated cross section of both components. When the angular distributions are not isotropic, one can take a constant equal to the minimum value of $d\sigma/d\theta$ as an upper limit for the compound nucleus cross sections. These angle-integrated charge distributions are displayed in Fig. 9.

The non isotropic components which we have identified as quasi and deep inelastic reactions are concentrated in the general neighborhood of the target and projectile. This is particularly true for the ^{12}C target. However, due to the less asymmetric entrance channel of the $^{63}Cu + ^{27}Al$ reaction, the deep inelastic component is present for almost the entire Z-range of products. In general, for both targets the isotropic component is larger for intermediate Z-values, while the deep-inelastic component is larger near the projectile and target Z-values.

The isotropic component from the $^{63}Cu + ^{12}C$ reaction shows the characteristic U-shaped pattern which we have now learned to associate with the decay of compound systems below the Businaro-Gallone point. For the $^{63}Cu + ^{27}Al$ system, the

Z-distribution is much flatter. This flattening of the shape of the charge distribution is due to the larger excitation energy and angular momentum associated with the latter system. The yields of the isotropic component for the $^{63}Cu + ^{27}Al$ system are generally more than an order of magnitude larger than those for the $^{63}Cu + ^{12}C$ system. This large increase in yield is due both to the larger excitation energy and larger angular momentum available in the compound system formed in the $^{63}Cu + ^{27}Al$ reaction.

The predicted compound nucleus cross sections, of course, depend strongly on the energy dependent branching ratios between complex fragment emission and light particle emission. Consequently, the experimental absolute cross sections contain the strongest information regarding the mechanism of complex fragment emission. In order to verify the compound nucleus hypothesis we have fitted the data with the Monte Carlo code Gemini,[16] which, beside treating light fragment evaporation in a conventional way, specifically allows compound nuclei to decay by complex fragment emission. Every fragment produced in the decay is followed until all of the available excitation energy is exhausted.

Crucial ingredients of these calculations are the angular-momentum-dependent conditional barriers as a function of mass asymmetry. These barriers have been calculated with the finite range model developed by Sierk.[25] The calculated saddle plus rotational energies are shown as a function of mass asymmetry and angular momentum in Fig. 10 for the reaction $^{63}Cu + ^{27}Al$. These barriers are almost identical with those from the reaction $^{63}Cu + ^{12}C$. For low partial waves, the calculated barriers show a maximum at symmetry, in accordance with the fact that the system is below the Businaro-Gallone point. As the angular momentum increases the barriers becomes flatter and flatter around the symmetry point. Eventually a minimum develops by $\ell = 60\hbar$. This is due to the dependence of the Businaro-Gallone point on angular momentum. Clearly for $\ell = 60\hbar$, the system is above the Businaro-Gallone point.

For the system $^{63}Cu + ^{12}C$, a maximum angular momentum of $\ell \cong 40\hbar$ is expected from the Bass model[26,27]. Consequently, the resulting charge distribution should be U-shaped, namely with a minimum at symmetry where the barriers are higher (see Fig.

10).

For the system $^{63}Cu + ^{27}Al$, the calculated[26] maximum angular momentum is $\ell \cong 70\hbar$, well above the Businaro-Gallone value. Therefore, a rather flat distribution should be expected with the possibility of a weak minimum or peaking at symmetry depending on the relative contributions from the low and high partial waves to the cross section.

The only parameter used in fitting the data was the maximum angular momentum. The fit to the charge distribution for $^{63}Cu + ^{12}C$ system is shown in Fig. 11. The quality of the fit is acceptable, except for fluctuations in the lighter element cross sections partly due to poor Monte Carlo statistics, partly due to difficulties in handling sequential decay by the code. The extracted maximum angular momentum should correspond to the fusion cross section. The Bass model[26,27] predicts $\ell_{max} = 39\hbar$, while we obtain $\ell_{max} = 31\hbar$ from the fit to the data, which is somewhat lower than expected. Considering that the absolute cross sections could have a systematic error of up to 30%, the agreement is satisfactory.

In the case of the $^{63}Cu + ^{27}Al$ reaction, we need to sum the cross sections up to $\ell_{max} = 66\hbar$ in order to reach the experimental cross sections (see Fig. 12). The Bass model[26,27] predicts $\ell_{max} = 68\hbar$. The increase in the experimental charge distribution of over a factor of 50 relative to the $^{63}Cu + ^{12}C$ system and the change in the shape from a U-shaped to a flat distribution is adequately reproduced. The reason why there is better agreement with the Bass model prediction of ℓ_{max} for the $^{63}Cu + ^{27}Al$ than for the $^{63}Cu + ^{12}C$ reaction is not clear at the moment. Hopefully, this can be understood when extensive excitation functions for both reactions become available.

One should note that GEMINI predicts that the evaporation residues (dashed lines in Figs. 11 & 12) are the dominant fusion products in the $^{63}Cu + ^{12}C$ system, whereas the binary decay products are dominant fusion products for the $^{63}Cu + ^{27}Al$ system. As the compound nucleus is produced with larger excitation energy and angular momentum, the fusion yield appears as binary decay products.[19] At even larger

energies and angular momentum, one might expect 3- & 4-body sequential decay products to be abundantly produced from compound nuclei.

3.5 Coincidence Data

The coincidence data confirm the finding from the singles data that the process is essentially binary in nature. The Z_1 vs Z_2 distributions for the $^{63}Cu + ^{12}C$ and $^{63}Cu + ^{27}Al$ systems are given in Fig. 13, where Z_1 and Z_2 are the atomic numbers of the two fragments in coincidence. All the coincidence events lie in a narrow region of the Z_1 - Z_2 plane, quite close to the sum of the target and projectile Z values. In both systems, peaks in the general vicinity of the target and projectile are observed which are associated with quasi and deep inelastic reactions. However, the distribution of events within the band of approximately constant $Z_1 + Z_2$ has no immediate significance because it is strongly biased by the relative and absolute positions of the two detectors. The effect of the detector geometry on the coincidence yield is shown in Fig. 14, where different detector positions have been selected. The main conclusion that one can draw from these graphs is the approximate constancy of the sum $Z_1 + Z_2$.

The $Z_1 + Z_2$ spectra for the two reactions are shown in Fig. 15. The relatively sharp peaks positioned near the total charge of the system again indicate the binary nature of the reaction. Similar features are shown by the corresponding spectra calculated with the GEMINI code, although the experimental spectra are somewhat broader than the calculations. The narrowness of the peaks implies a weak dependence of the sum $Z_1 + Z_2$ upon the charge of one of the fragments. This is seen more explicitly by the dependence of the sum of the average charges $\langle Z_1 + Z_2 \rangle$ on one of the fragment's charge Z_1 shown in Fig. 16. The independence of $\langle Z_1 + Z_2 \rangle$ on the atomic number Z_1 of one fragment strongly suggests that the complex fragments measured in coincidence originate from the same process, and most likely from the decay of the same compound nucleus.

For $^{63}Cu + ^{12}C$ system the peak of the $Z_1 + Z_2$ distribution is located at about 32.3, while the peak is at 36.7 for $^{63}Cu + ^{27}Al$ reaction. The atomic numbers of the

corresponding compound nuclei are 35 and 42. The difference between the measured sum $Z_1 + Z_2$ and the compound nucleus atomic number can be attributed to light charged particle evaporation before and after the major binary decay. The charge lost is about 3 for $^{63}Cu + ^{12}C$ reaction, whereas it is about 5 for $^{63}Cu + ^{27}Al$ reaction.

Light particle evaporation strongly depends on the excitation energy of the compound system. The calculated excitation energies are about 132 MeV and 234 MeV for reactions using ^{12}C and ^{27}Al targets, respectively. The ratio of these excitation energies is quite close to the ratio of 5/3 for the charge lost in $^{63}Cu + ^{27}Al$ reaction to that in $^{63}Cu + ^{12}C$ reaction. Thus it appears that the charge lost is approximately proportional to the excitation energy[24] as expected from the statistical decay theory. More quantitatively one can compare the average $\langle Z_1 + Z_2 \rangle$ calculated from the GEMINI code with the experimental data. This is shown by the line in Fig. 16. The agreement between the calculations and the data is excellent for both reactions. Naturally this comparison proves only that one has observed full energy relaxation, which is true both for compound nucleus and deep inelastic reactions.

The binarity of the events is vividly portrayed by the the distribution of the c.m. angle between the two fragments shown in Fig. 17. The distributions peak at 180° as expected for back-to-back emission of complex fragments in a binary decay process. The width of the peaks is due to the recoil associated with secondary emission of light particles.

The experimental total kinetic energies (solid symbols) of the fragment pairs in the center-of-mass frame are illustrated in Fig. 18. The observed symmetric distribution with a peak at symmetry is characteristic of the Coulomb energy between one fragment and its partner. The fluctuations (open symbols) in the average total kinetic energies, also shown in the figure, are partly due to recoil effects associated with secondary decays, partly are primary and are due to shape fluctuations that affect the Coulomb repulsion. The dashed curves shown in the figures are based upon a generalization of the Viola systematics[20] for fission fragments to all mass asymmetries. The solid curves include also the kinetic energies associated with the average orbital angular momentum. The effect of sequential evaporation has been accounted for in an approximate way. The agreement is excellent for the Cu + Al reaction, while the

calculated kinetic energies are somewhat lower than the experiment for the Cu + C reacion. The origin of this minor discrepancy is unclear.

4. Conclusions

The main conclusion of this work is that in both reactions complex fragments arise from the binary decay of a single source with complete fusion velocity. The reaction mechanisms involved are quasi-elastic and deep-inelastic reactions from products near the target and projectile, and compound nucleus decay for products covering the entire atomic number range. The two components can be easily separated for the $^{63}Cu + ^{12}C$ reaction, but not quite as easily for the $^{63}Cu + ^{27}Al$ reaction due to more extensive contamination from deep inelastic reactions. A compound nucleus calculation reproduces the absolute cross sections of the isotropic binary decay component as a function of Z value for both systems.

Acknowledgment

This work was supported by the Director, Office of Energy Research, Division of Nuclear Physics of the Office of High Energy and Nuclear Physics of the U. S. Department of Energy under Constract DE-AC03-76SF00098.

References

1. L. G. Moretto and G. J. Wozniak, Prog. in Part. & Nucl. Phys. **21** (1988).
2. L. G. Moretto, M. Ashworth, and G. J. Wozniak, Proc. of the 8th High Energy Heavy Ion Study, Nov. 16-20, 1987. LBL- 24580 , p. 273 (1988).
3. L. G. Moretto and G. J. Wozniak, Proc. of the 3rd Int'l Conf. on Nucl. - Nucl. Coll., St. Malo, (1988), LBL-25322.
4. L. G. Moretto and G. J. Wozniak, Proc of the Sapporo Int'l Symp., Sapporo, Japan (1988), LBL-25631.
5. W. U. Schröder and J. R. Huizenga, Ann. Rev. Nucl. Sci. **27** (1977) 465.
6. L. G. Moretto and R. P. Schmitt, J. Phys. **37C5** (1976) 109
7. L. G. Moretto and G. J. Wozniak, Ann. Rev. Part. Sci. **34** (1984) 189
8. B. Shivakumar, D. Shapira, P. H. Stelson, S. Ayik, B. A. Harmon, K. Teh, and D. A. Bromley, Phys. Rev. **C37**, (1988) 652.
9. A. Olmi, P. R. Maurenzig, A. A. Stefanini, J. Albinski, A. Gobbi, S. Gralla, N. Herrmann, K. D. Hildenbrand, J. Kuzminski, W. F. J. Müller, M. Petrovici, H. Stelzer, and J. Toke, Europhys. Lett. **4**, 1121 (1987). A. Olmi, Proc. of the 8th High Energy Heavy Ion Study, LBL-24580 (1988) 288.
10. B. Borderie, M. Montoya, M. F. Rivet, D. Jouan, C. Cabot, H. Fuchs, D. Gardes, H. Gauvin, D. Jacquet, F. Monnet, and F. Hanappe, Phys. Lett. **205** (1988) 26.
11. L. G. Sobotka, M. L. Padgett, G. J. Wozniak, G. Guarino, A. J. Pacheco, L. G. Moretto, Y. Chan, R. G. Stokstad, I. Tserruya, and S. Wald Phys. Rev. Lett. **51** (1983) 2187.
12. M. A. McMahan, L. G. Moretto, M. L. Padgett, G, J. Wozniak, L. G. Sobotka, and M. G. Mustafa, Phys. Rev. Lett. **54** (1985) 1995.
13. R. J. Charity, M. A. McMahan, D. R. Bowman, Z. H. Liu, R. J. McDonald, G. J. Wozniak, L. G. Moretto, S. Bradley, W. L. Kehoe, A. C. Mignerey, and M. N. Namboodiri, Phys. Rev. Lett. **56** (1986) 1354.
14. D. R. Bowman, W.L. Kehoe, R. J. Charity, M. A. McMahan, A. Moroni, A. Bracco, S. Bradley, I. Iori, R. J. McDonald, A. C. Mignerey, L. G. Moretto, M. N. Namboodiri, and G. J. Wozniak, Phys. Lett. **B189** (1987) 282.

15. R. J. Charity, D. R. Bowman, Z. H. Liu, R. J. McDonald, M. A. McMahan, G. J. Wozniak, L. G. Moretto, S. Bradley, W. L. Kehoe, and A. C. Mignerey, Nucl. Phys. **A476** (1988) 516.
16. R. J. Charity, M, A. McMahan, G. J. Wozniak, R.J. McDonald, L. G. Moretto, D. G. Sarantites, L.G. Sobotka, G. Guarino, A. Pantaleo, L. Fiore, A. Gobbi and K. Hildenbrand, Nucl. Phys. **A483** (1988) 371.
17. J. Gomez del Campo, J. L. Charvet, A. D'Onofrio, R. L. Auble, J. R. Beene, M. L. Halbert and H. J. Kim, Phys. Rev. Lett. **61** (1988) 290.
18. L. G. Sobotka, M. A. McMahan, R. J. McDonald, C. Signarbieux, G. J. Wozniak, M. L. Padgett, J. H. Liu, Z. Q. Yao and L. G. Moretto, Phys. Rev. Lett. **53** (1984) 2004.
19. E. Plagnol, L. Vinet, D. R. Bowman, Y. D. Chan, R. J. Charity, E. Chavez, S. B. Gazes, H. Han, W. L. Kehoe, M. A. McMahan, L. G. Moretto, R. G. Stokstad, and G. J. Wozniak, Lawrence Berkeley Laboratory preprint # LBL-25742.
20. V. E. Viola, K. Kwiatkowski, and M. Walker, Phys. Rev. **C31**, (1985) 1550.
21. G. J. Mathews, J. B. Moulton, G. J. Wozniak, B. Cauvin, R. P. Schmitt, J. S. Sventek, and L. G. Moretto, Phys. Rev. **C25**, (1982) 300.
22. L. G. Moretto, S. K. Kataria, R. C. Jared, R. Schmitt, and S. G. Thompson, Nucl. Phys. **A255** (1975) 491.
23. R. Babinet, L. G. Moretto, J. Galin, R. Jared, J. Moulton and S. G. Thompson, Nucl. Phys. **A258** (1976) 172.
24. R. P. Schmitt, G. Bizard, G. J. Wozniak and L. G. Moretto, Phys. Rev. Lett. **46** (1981) 522.
25. A. J. Sierk, Phys. Rev. **C33**, (1986) 2039.
26. R. Bass, Nucl. Phys. **A231** (1974) 45.
27. R. Bass, Phys. Rev. Lett. **39** (1977) 265.

Figure Captions

1. Schmetic ridge line potentials (solid curves) and expected yields (dashed curves) as a function of the mass asymmetry coordinate for: a) a heavy system above and (b) a light system below the Businaro-Gallone point.
2. Schematic diagram showing the relative overlap of contributions from different processes as the function of the product Z-value in a heavy ion reactions for a light and heavy system.
3. Density plot of ΔE - E for the reaction 12.6 MeV/nucleon ^{63}Cu + ^{12}C for fragments detected at forward laboratory angles.
4. Contour plots of the invariant cross section ($\partial^2\sigma/V^2\partial V\partial Z$) in the Z-V plane for fragments from the 12.6 MeV/nucleon ^{63}Cu + ^{12}C reaction detected at four different angles. To minimize the kinematic broadening, an angular gate of one degree in width has been set for each angle shown.
5. Contours of the experimental cross section $\partial^2\sigma/\partial V_{\parallel}\,\partial V_{\perp}$ in the $V_{\parallel}$ -$V_{\perp}$ plane for representative fragment Z-values detected in the reaction E/A = 12.6 MeV/A ^{63}Cu + ^{12}C reaction. The beam direction is vertical. The dashed lines show the maximum and minimum angular thresholds and the velocity threshold of the detector telescopes.
6. Same as for Fig. 5, for the E/A = 12.6 MeV ^{63}Cu + ^{27}Al reaction.
7. Source velocities extracted from the Coulomb velocity rings for each Z-species produced in the 12.6 MeV/A ^{63}Cu plus ^{12}C & ^{27}Al reactions. The small error bar on each point indicates the statistic error associated with the extraction process. The single large error bar for each data set indicates the possible systematic error due to the mass parameterization and energy calibrations. The beam and complete fusion velocities are also shown in the plot as horizontal lines. In the lower portion of the figure, are shown the extracted Coulomb velocities and widths. For comparison a calculation based on the Viola systematics[20] without (dashed line) and with angular momentum effects (solid line) is shown.
8. Representative angular distributions $d\sigma/d\theta$ in the frame of the source system for the E/A=12.6 MeV ^{63}Cu+^{12}C & ^{27}Al reactions. The solid lines are to

guide the eye.

9. Angle-integrated charge distributions of complex fragments associated with compound nucleus (open symbols) and deep inelastic (filled symbols) processes for the 12.6 MeV/A ^{63}Cu + ^{12}C,^{27}Al reactions.
10. Calculated saddle plus rotational energies are shown as a function of mass asymmetry and angular momentum for the reaction ^{63}Cu + ^{27}Al.
11. Comparison of experimental and calculated charge distributions for the ^{63}Cu + ^{12}C reaction. The experimental data are indicated by the dots and the calculated values are shown by the error bars. The dashed line corresponds to the calculated yield of classical evaporation residues, which have not emitted a particle heavier than an alpha particle.
12. Comparison of experimental and calculated charge distributions for the ^{63}Cu + ^{27}Al reaction (see Fig. 11).
13. Representative Z_1 - Z_2 contour plots for coincidence events from the reactions E/A = 12.6 MeV ^{63}Cu + ^{12}C & ^{27}Al. Z_1 and Z_2 refer to the Z-values of fragments detected in the two quad detectors (1 & 2) on opposite sides of the beam. The inserts show the detector geometry and the angular range covered.
14. For the reaction ^{63}Cu + ^{12}C, Z_1 - Z_2 contours plots are shown for coincidence events between one specific telescope in quad unit 1 and any telescope in quad unit 2. The inserts show the angular range covered. This figure shows the dependence of the coincidence yield on the detector geometry.
15. The relative yield of coincidence events plotted as a function of the sum of the atomic charges of the two coincident fragments for the ^{63}Cu + ^{12}C & ^{27}Al reactions. The solid curve was calculated with the evaporation code GEMINI.[16] The vertical arrows indicate the atomic numbers of the compound nuclei.
16. The mean sum $\langle Z_1+Z_2 \rangle$ of coincidence events plotted as a function of Z_1 for E/A = 12.6 MeV ^{63}Cu+^{12}C & ^{27}Al reactions. The bars indicate the variance of the sum distribution. The horizontal lines indicate the charges of the compound nuclei. The charge loss for binary events due to sequential evaporation was estimated using the evaporation code GEMINI[16] and residual Z_1 + Z_2 values are

indicated by the curved line.

17. Sum of the emission angles of fragment 1 and fragment 2 in the center-of-mass frame for E/A = 12.6 MeV ^{63}Cu on ^{12}C & ^{27}Al targets.

18. Total kinetic energies (solid symbols) and variances (open symbols) of the fragment pair in center-of-mass system for the E/A = 12.6 MeV ^{63}Cu plus ^{12}C & ^{27}Al reactions. The dashed lines are calculated using a generalization of the Viola systematics to asymmetric divisions, while the solid lines include also the kinetic energies associated with the average orbital angular momentum. The large error bars indicates the possible systematic uncertainty in the data due to the energy calibration and mass parameterization.

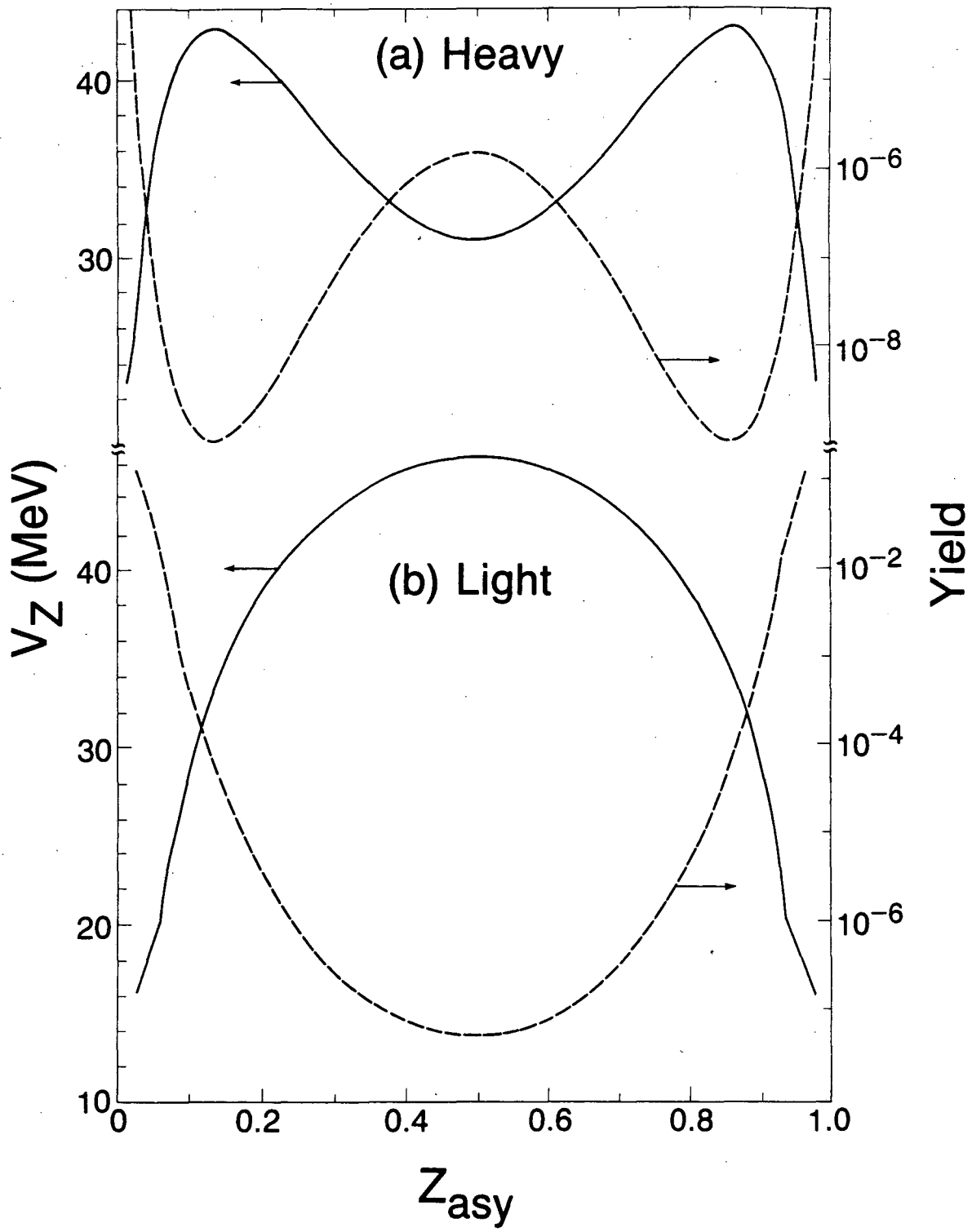

XBL 847-10685A

Figure 1

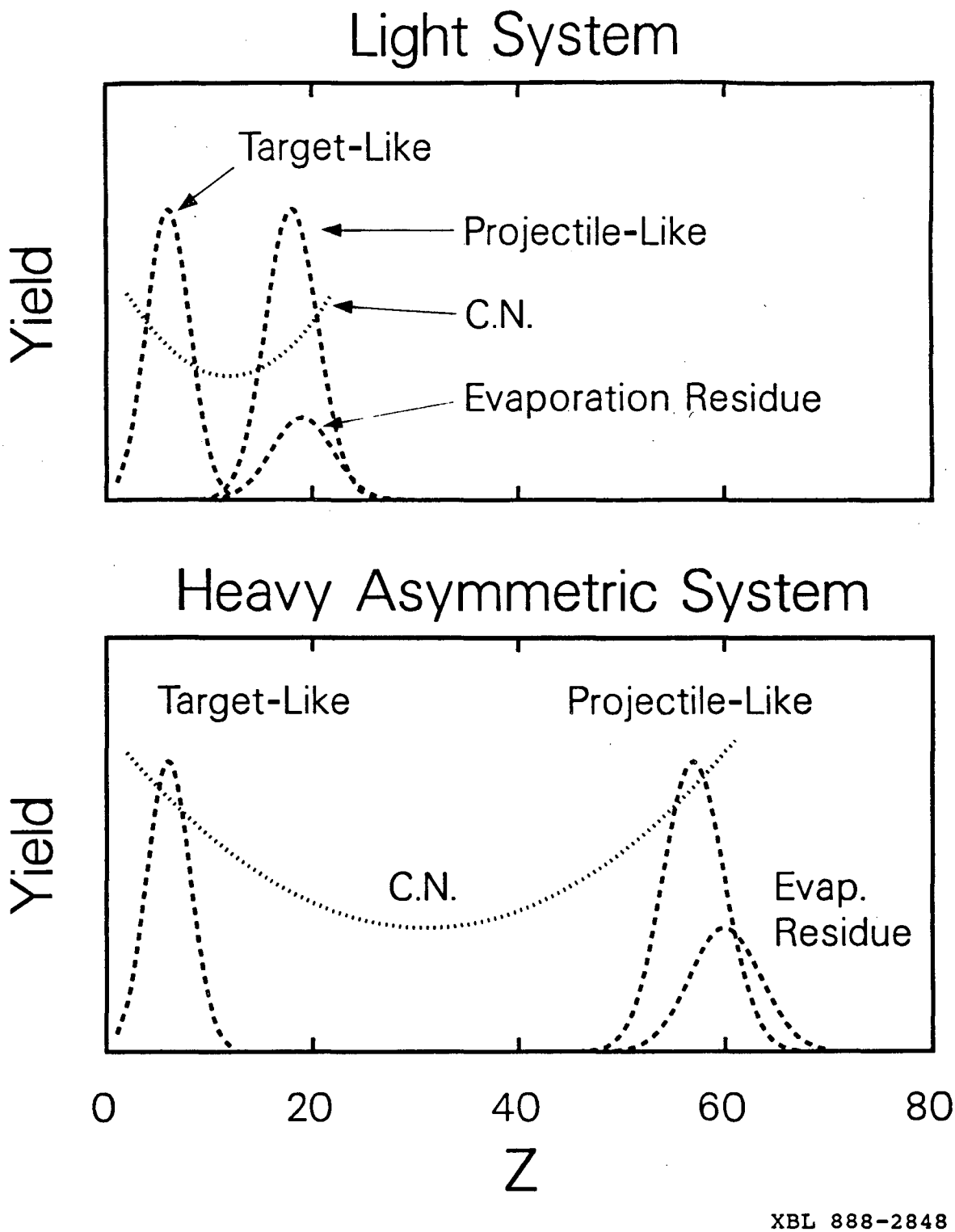

XBL 888-2848

Figure 2

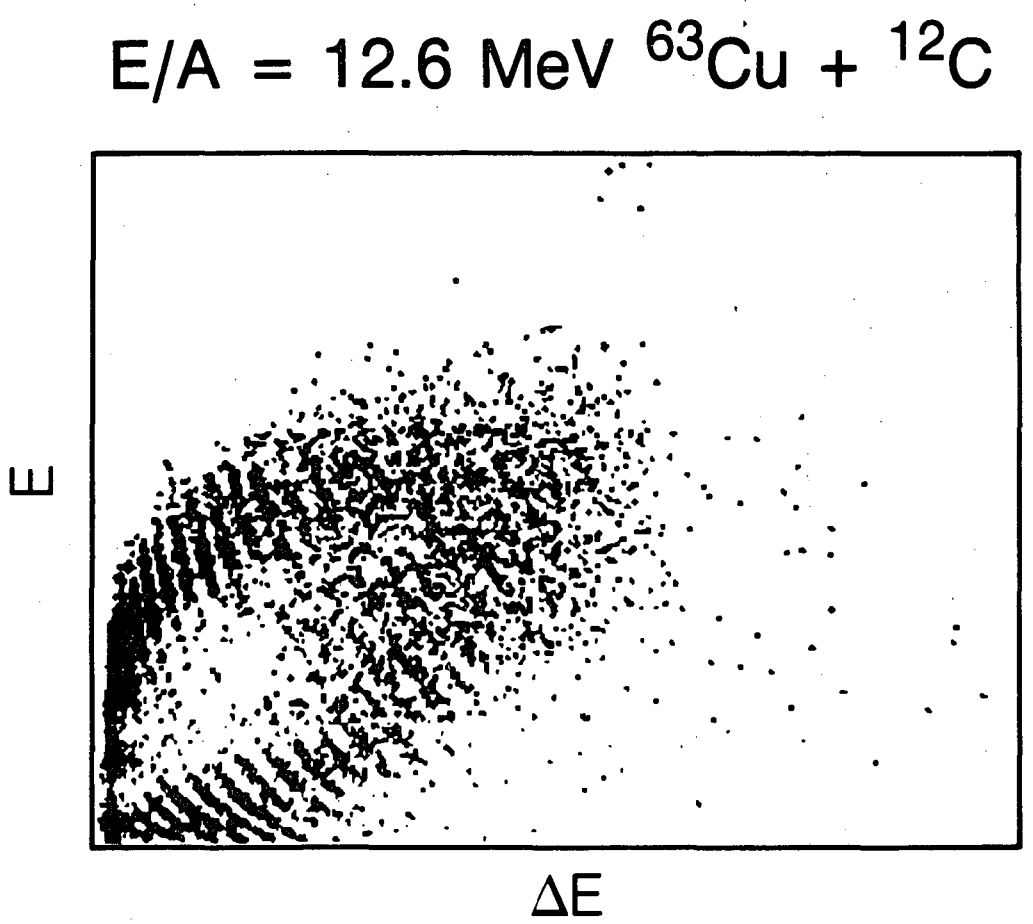

XBL 884-8034

Figure 3

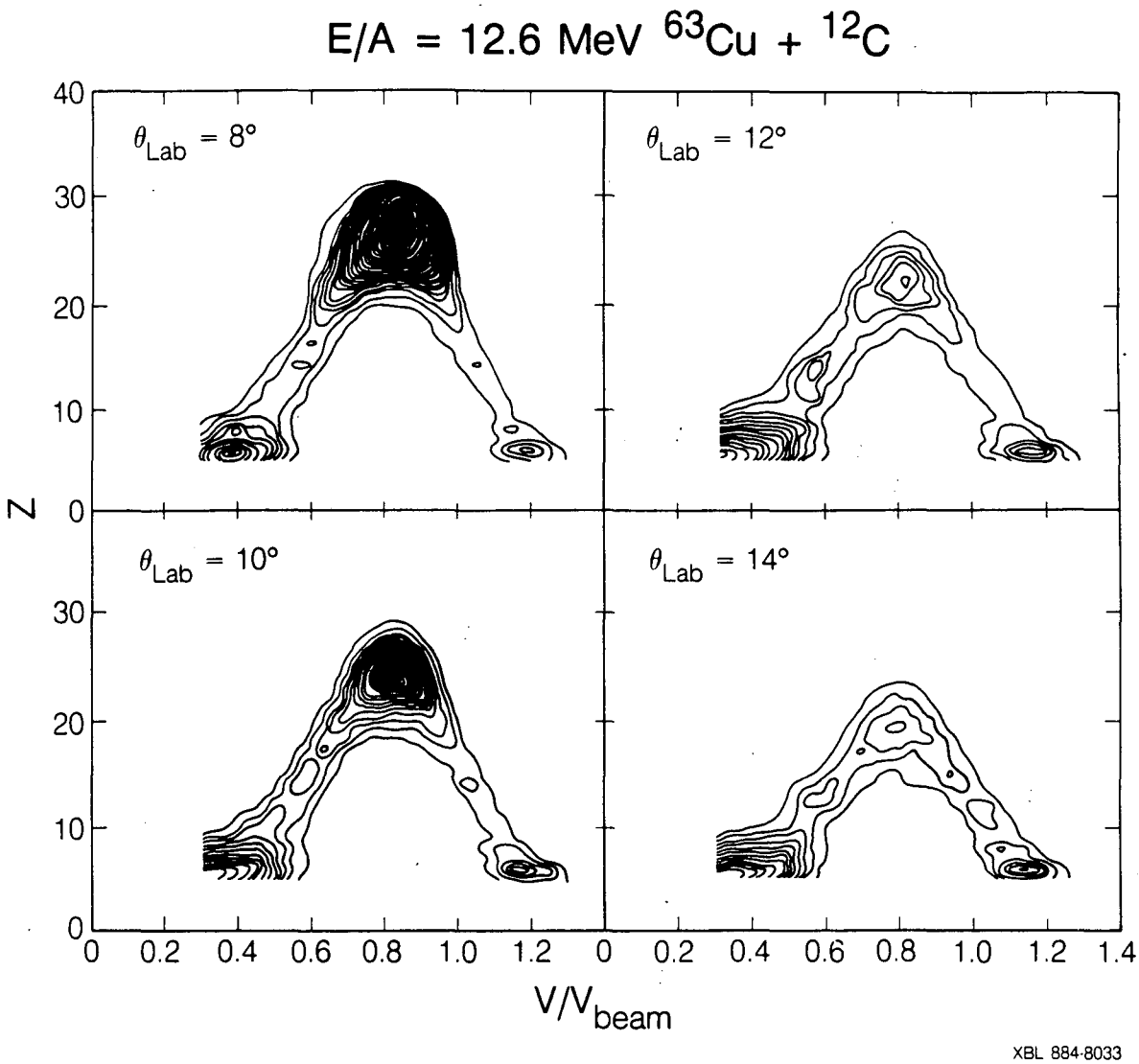
E/A = 12.6 MeV ^{63}Cu + ^{12}C
θ_{Lab} = 8°
θ_{Lab} = 12°
θ_{Lab} = 10°
θ_{Lab} = 14°
Z
V/V$_{beam}$
0
10
20
30
40
0.2
0.4
0.6
0.8
1.0
1.2
1.4
XBL 884-8033

Figure 4

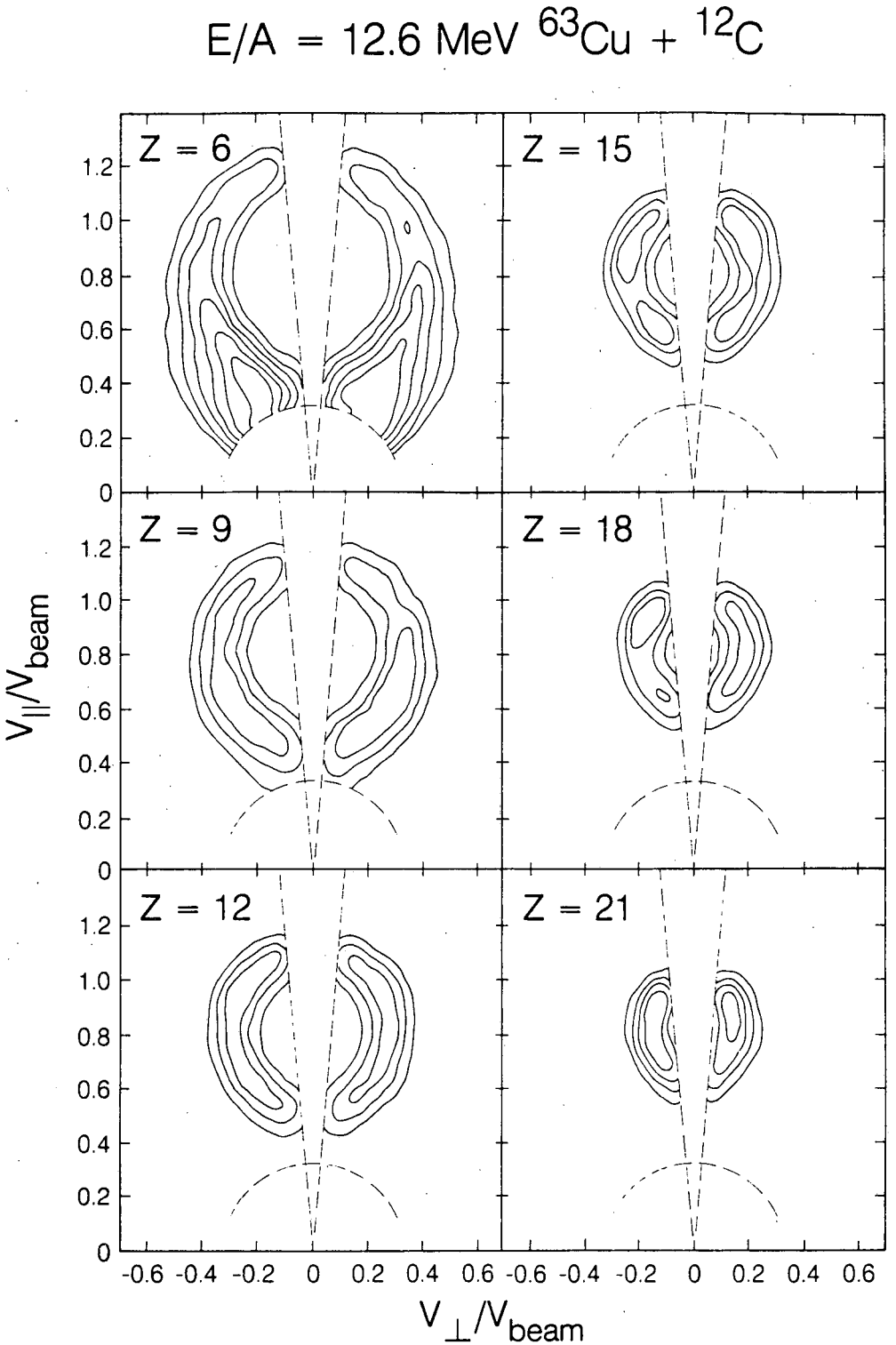
E/A = 12.6 MeV ^{63}Cu + ^{12}C
Z = 6
Z = 15
Z = 9
Z = 18
Z = 12
Z = 21
$V_{||}/V_{beam}$
$V_{\perp}/V_{beam}$
0
0.2
0.4
0.6
0.8
1.0
1.2
-0.6 -0.4 -0.2 0 0.2 0.4 0.6
XBL 881-8012

Figure 5

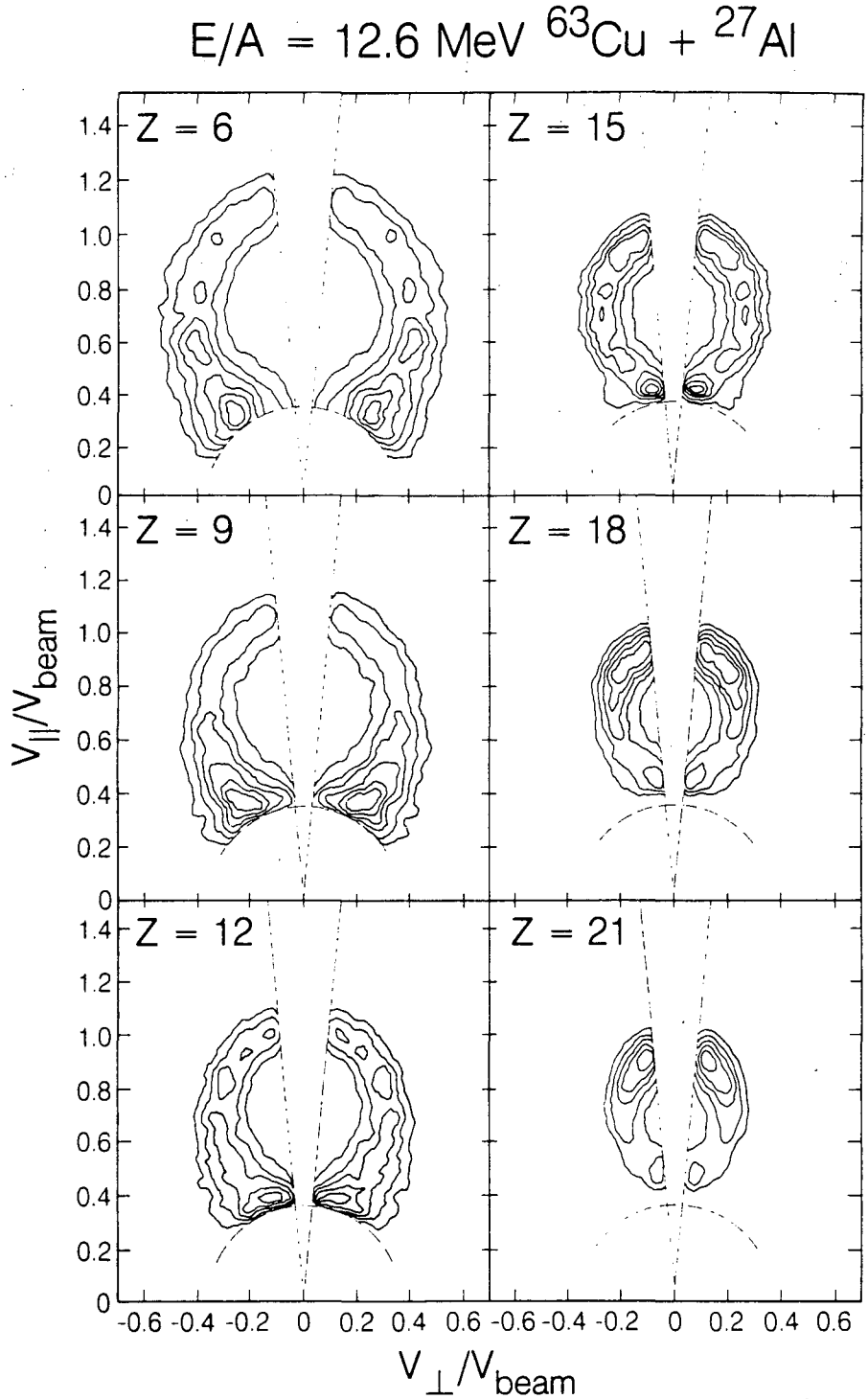

XBL 881-8008

Figure 6

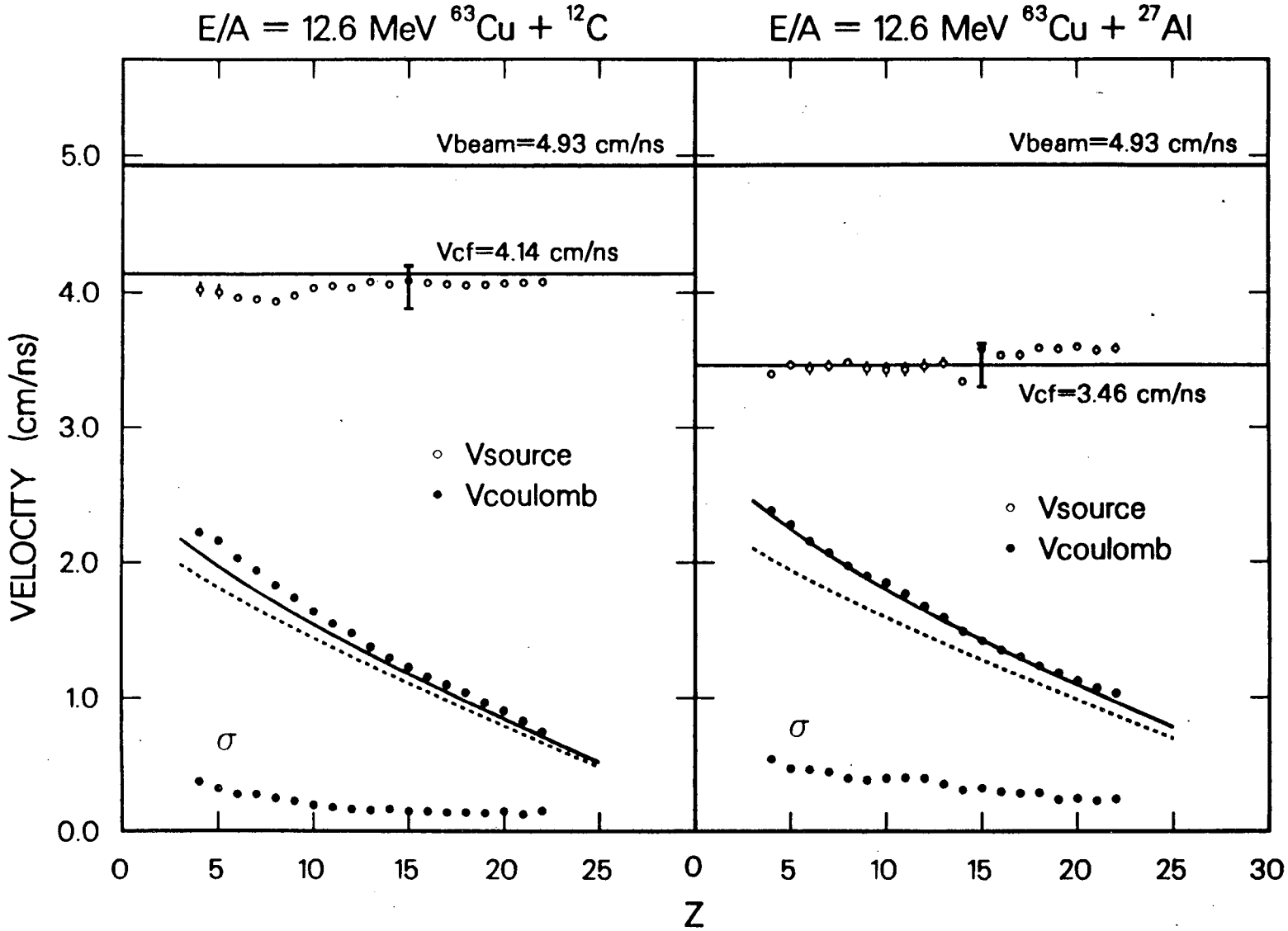

XBL 883-938

Figure 7

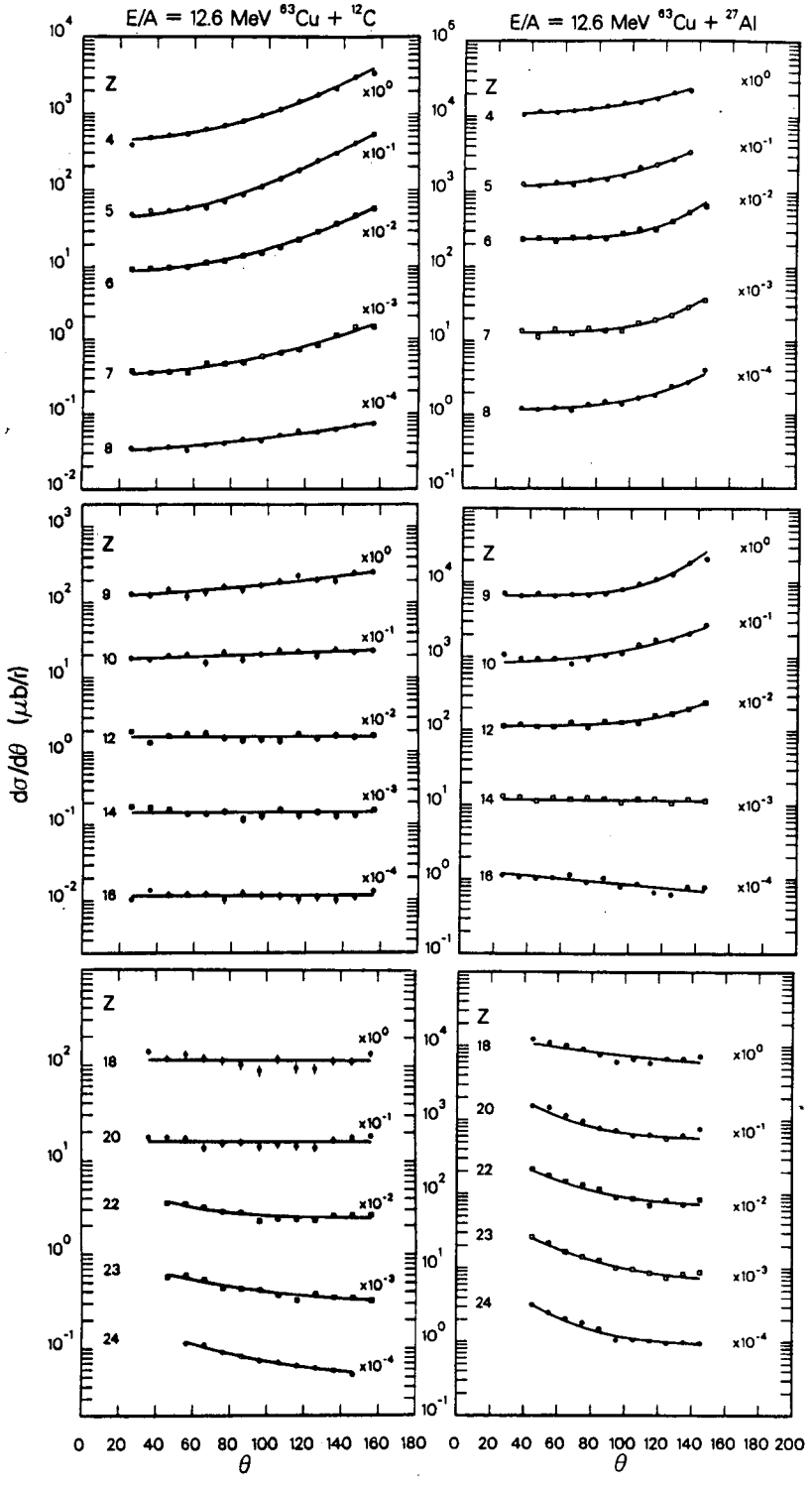

Figure 8

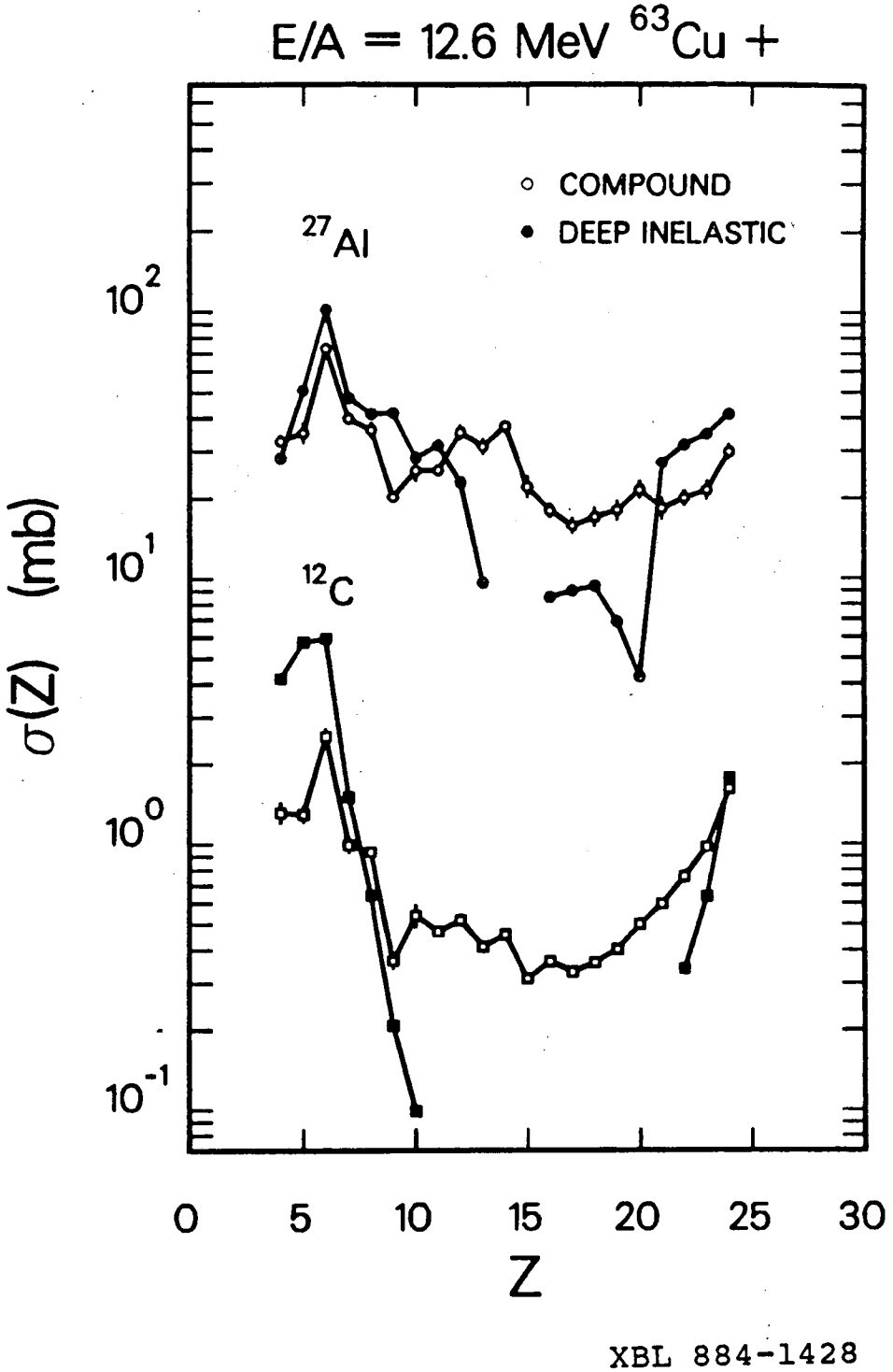
E/A = 12.6 MeV ^{63}Cu +
COMPOUND
DEEP INELASTIC
^{27}Al
^{12}C
10^2
10^1
10^0
10^{-1}
σ(Z) (mb)
0
5
10
15
20
25
30
Z
XBL 884-1428

Figure 9

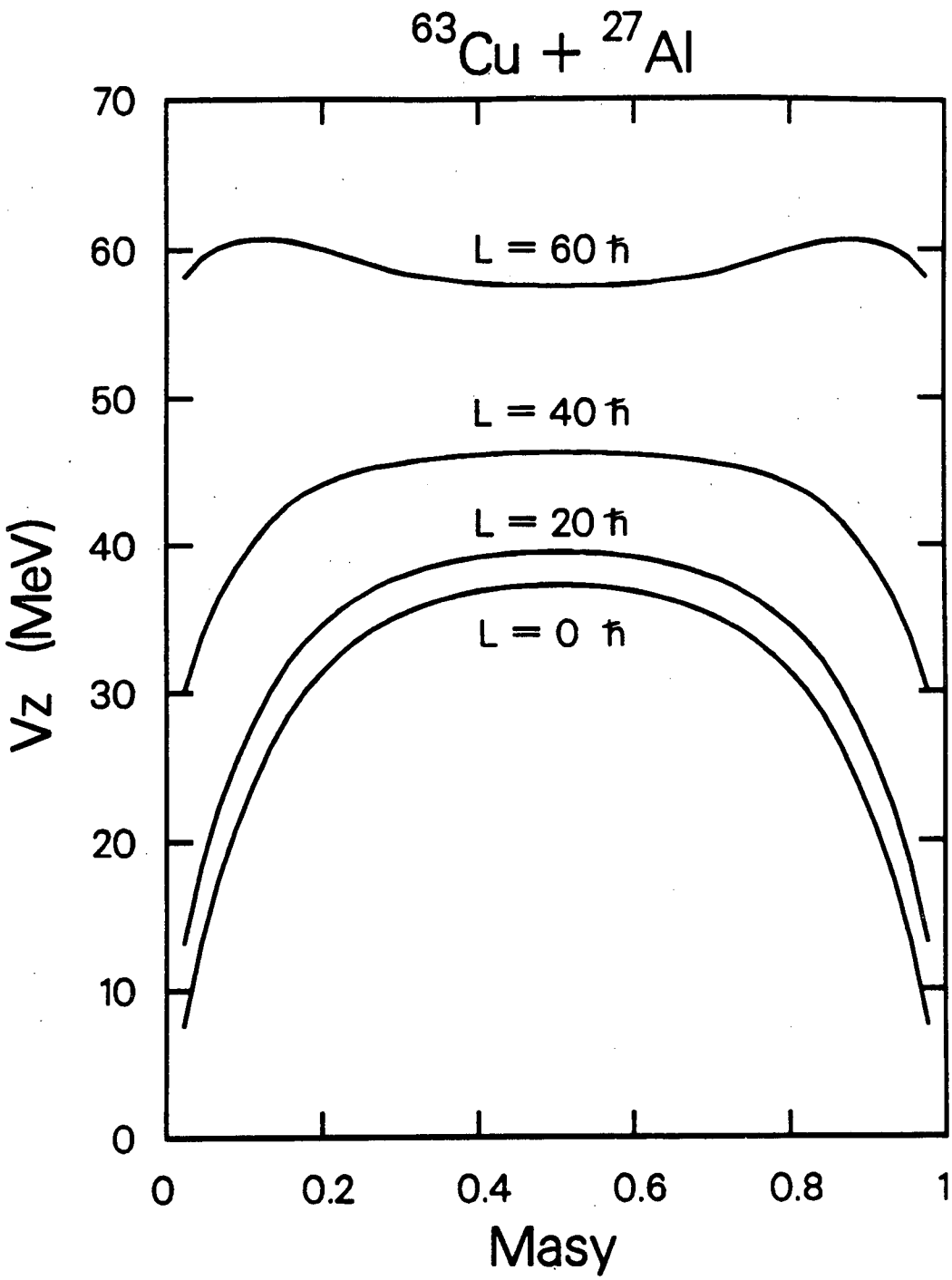

XBL 884-1430

Figure 10

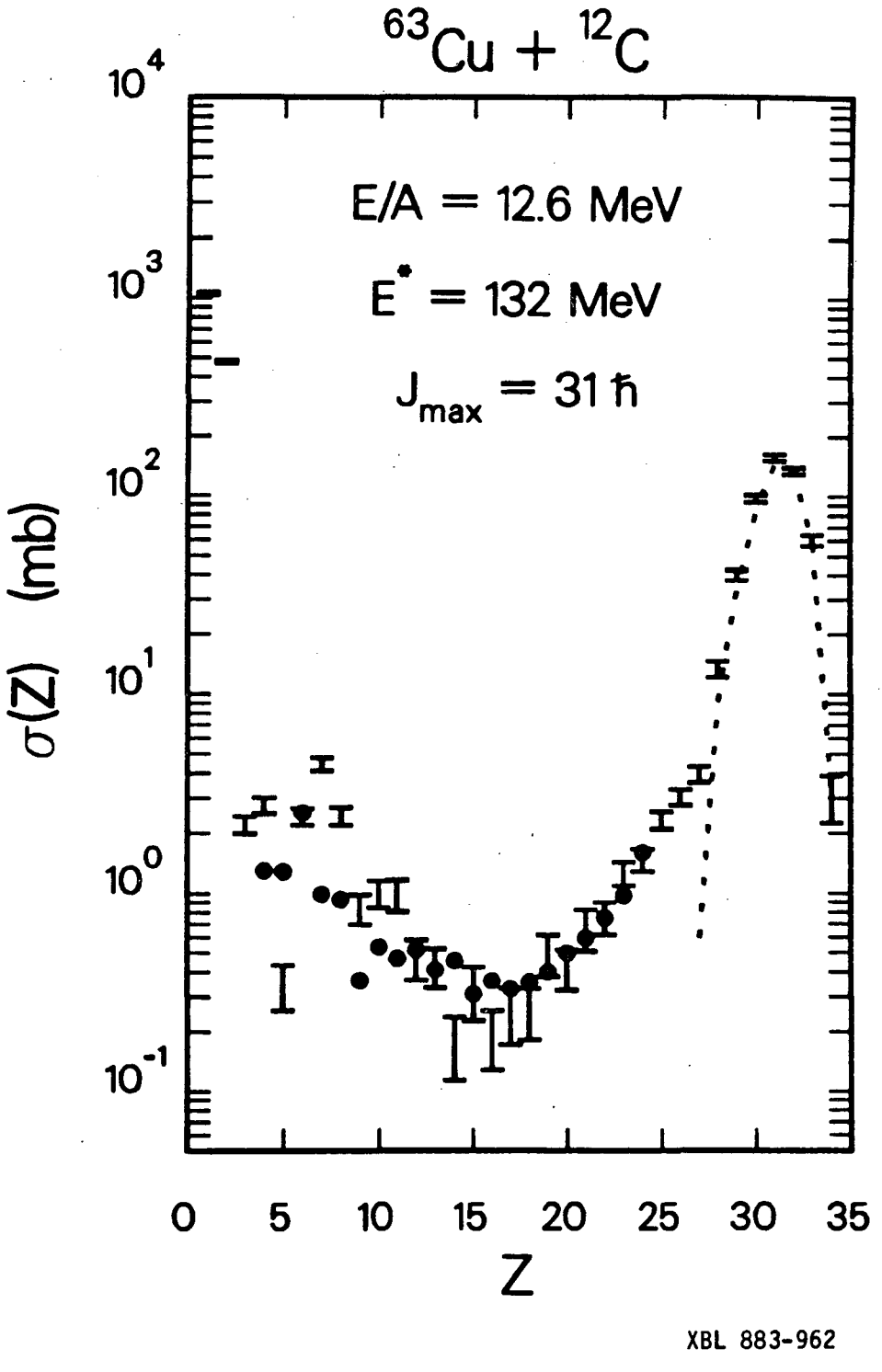

Figure 11

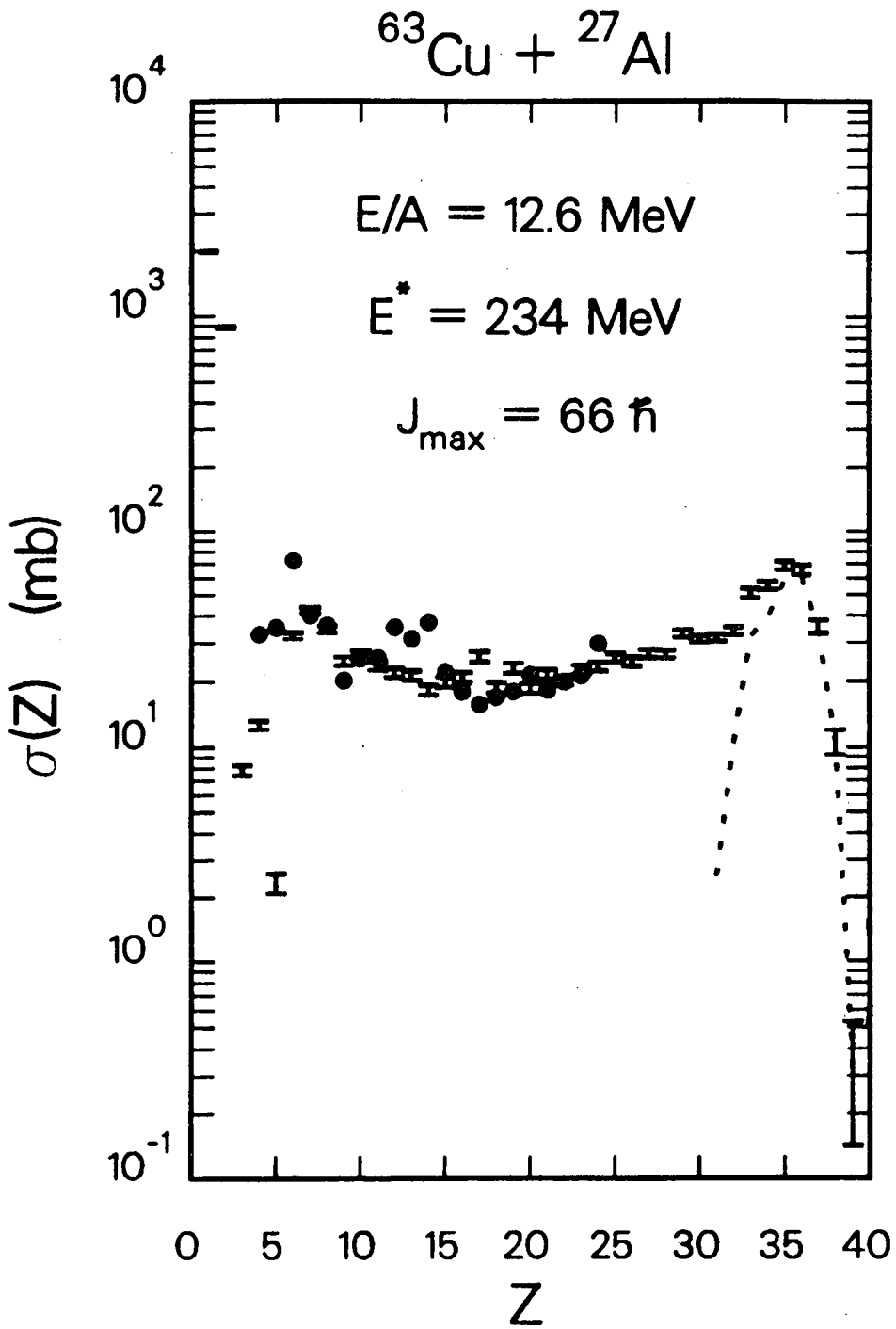

XBL 884-1427

Figure 12

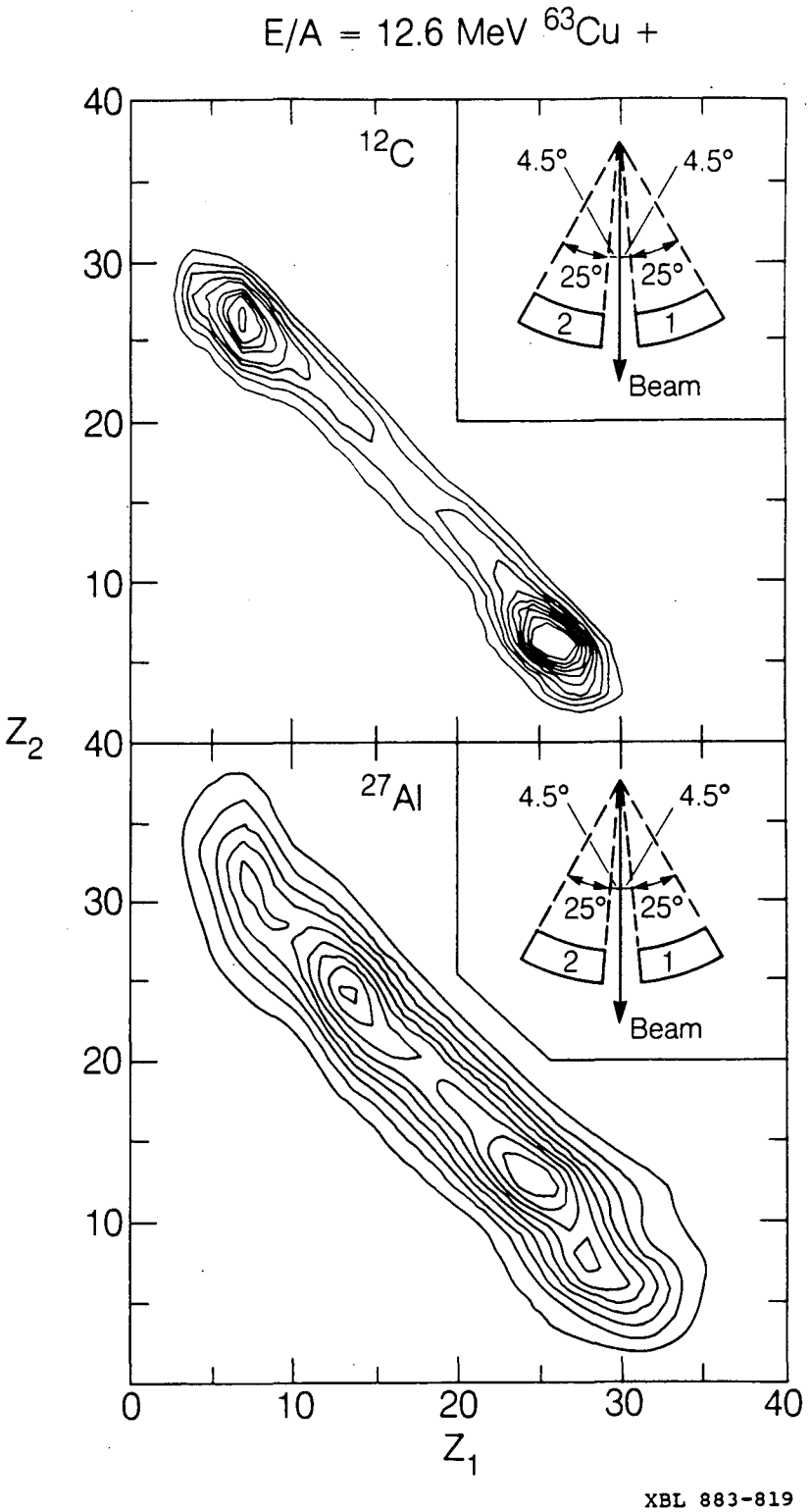
E/A = 12.6 MeV ^{63}Cu +
^{12}C
^{27}Al
4.5°
4.5°
25°
25°
2
1
Beam
Z_2
Z_1
0
10
20
30
40
XBL 883-819

Figure 13

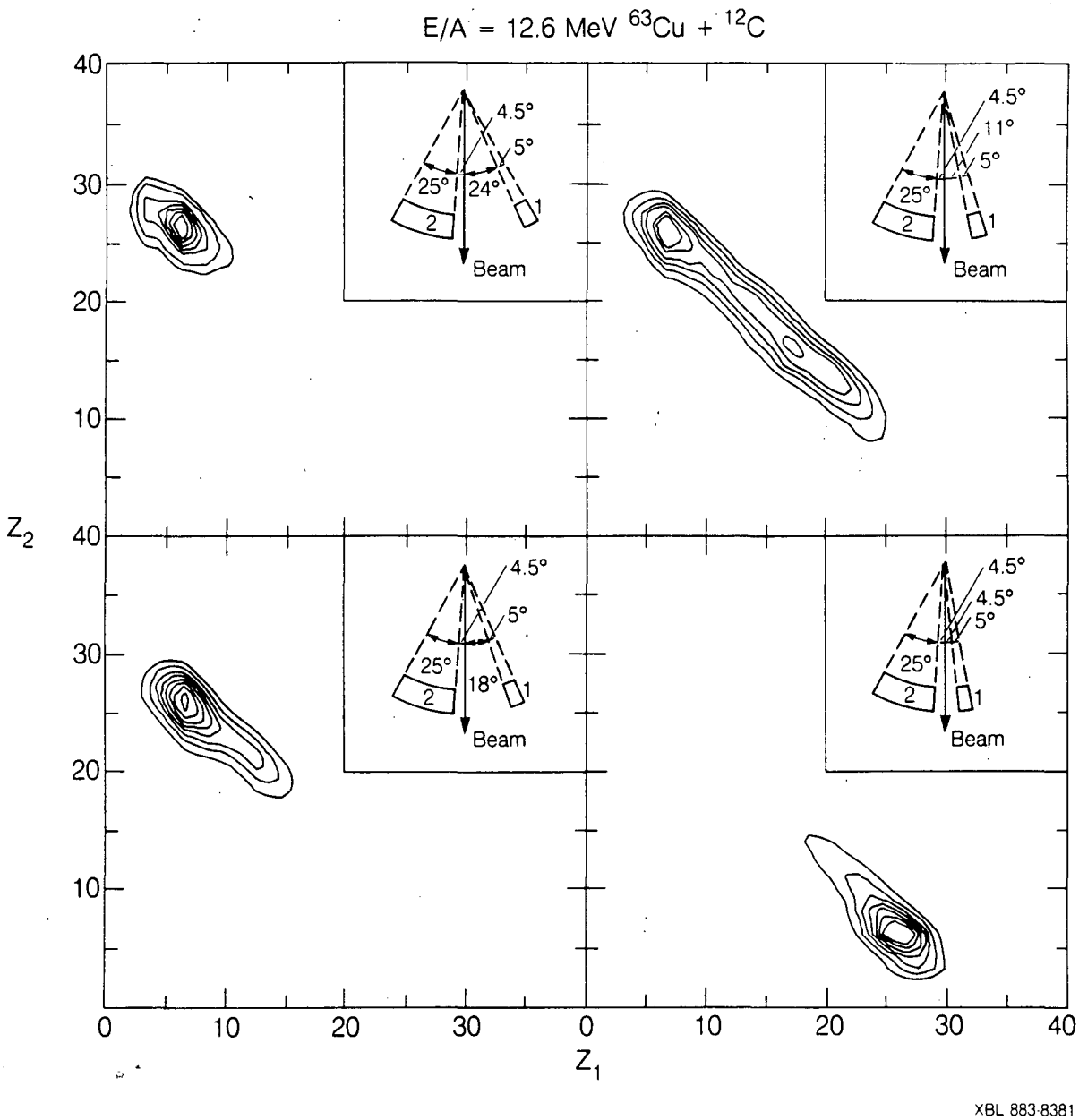
E/A = 12.6 MeV ^{63}Cu + ^{12}C
4.5°
5°
25°
24°
2
1
Beam
4.5°
11°
5°
25°
2
1
Beam
4.5°
5°
25°
18°
2
1
Beam
4.5°
4.5°
5°
25°
2
1
Beam
Z_2
Z_1
0
10
20
30
40
XBL 883-8381

Figure 14

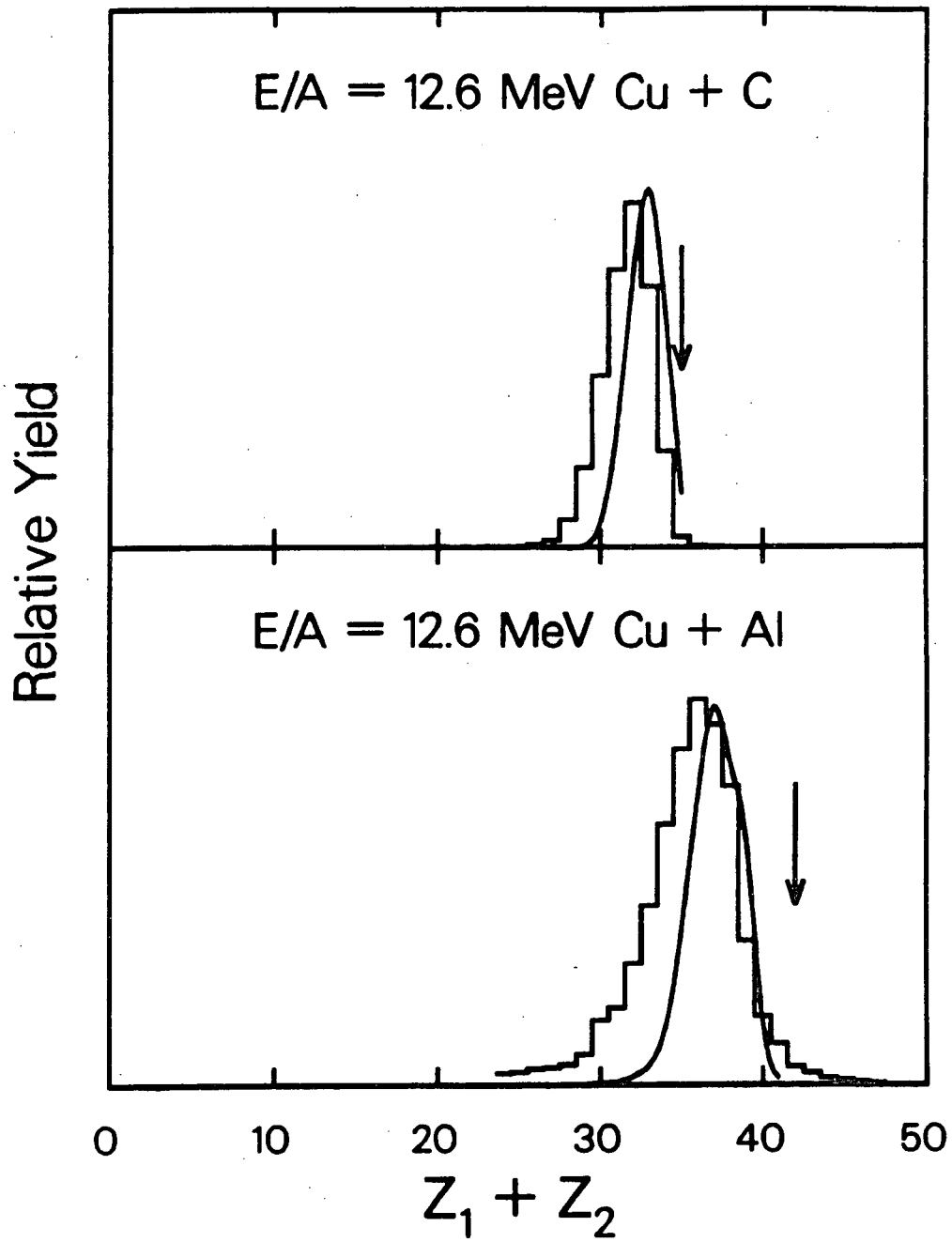

XBL 884-1429

Figure 15

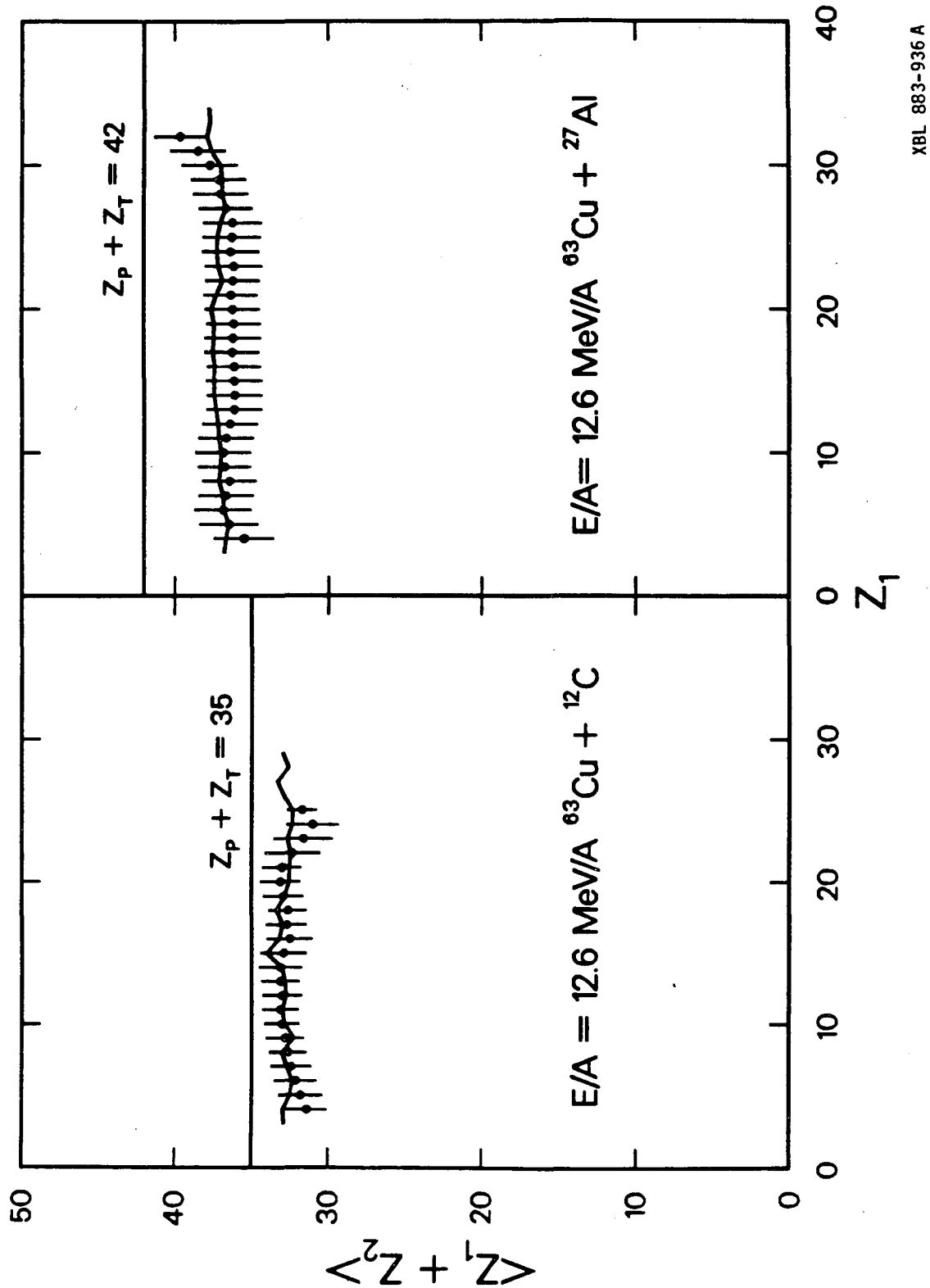

XBL 883-936 A

Figure 16

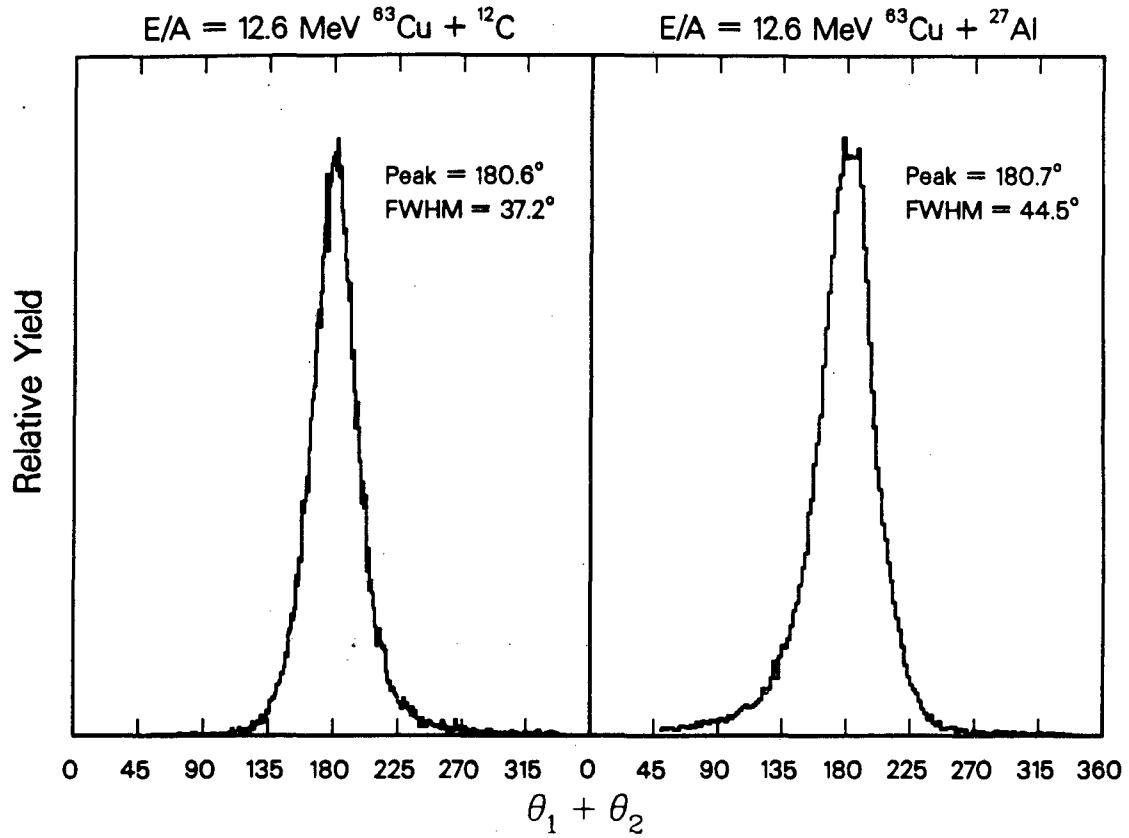

XBL 883-940

Figure 17

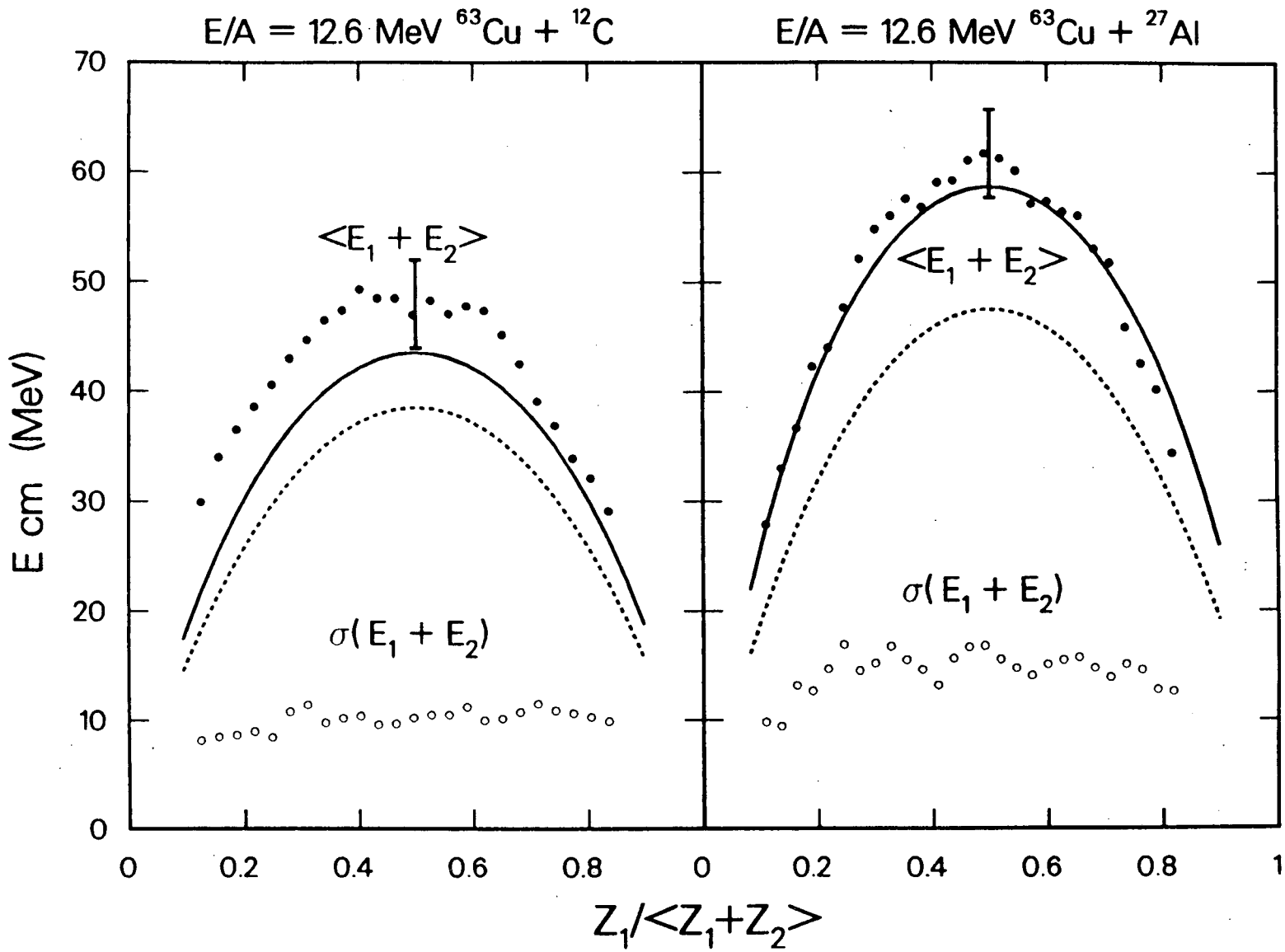

XBL 883-963

Figure 18

LAWRENCE BERKELEY LABORATORY
TECHNICAL INFORMATION DEPARTMENT
UNIVERSITY OF CALIFORNIA
BERKELEY, CALIFORNIA 94720